DOI: 10.1002/ejic.200701138

Microwave-Assisted Hydrothermal Synthesis of Structurally and Morphologically Controlled Sodium Niobates by Using Niobic Acid as a Precursor

Amauri J. Paula,*[a] Maria A. Zaghete,[a] Elson Longo,[a] and José A. Varela[a]

Keywords: Hydrothermal synthesis / Crystal growth / Niobates / Crystal morphology

There are many advantages to using a microwave as a source of heat in hydrothermal reactions. Because it is a quick and homogeneous way to crystallize ceramic powders, it was used in this work for the production of antiferroelectric sodium niobate ($NaNbO_3$) in a cubic-like form and its intermediary phase, disodium diniobate hydrate ($Na_2Nb_2O_6.H_2O$), with a fiber morphology. The syntheses were carried out by treating niobic acid ($Nb_2O_5{\cdot}nH_2O$) with NaOH. By changing the reaction time and the concentration of the reactants, particles with different structures and different morphologies could be obtained. The structural evolution of the products of this reaction was elucidated on the basis of the arrangement of the NbO_6 octahedral units. Conclusive results were obtained with morphological and structural characterizations through XRD, TEM, MEV, and NMR and Raman spectroscopy.

Introduction

The recent use of hydrothermal synthesis with the aim to obtain morphologically controlled particles opened a new and promising path in materials research. With the possibility to produce crystalline ceramic powders in a single process step that uses cheap apparatus and raw materials, this method has attracted the attention of the scientific community.[1] Because it is an environmentally friendly method, it can be used in manufacturing processes of a vast number of materials. Furthermore, different structural forms of the same compounds can be obtained with changes in the synthetic parameters, such as pH, temperature, raw material, or time.[2,3]

By associating microwave energy as source of energy with hydrothermal synthesis, many benefits can be achieved. Economy in costs as a result of the fast kinetic process, rapid heating, homogeneous crystallization, and differentiation in the products are only some of these gains.[4] Despite the benefits, there are still very few studies involving the use of this microwave-assisted hydrothermal method for the synthesis of perovskite oxides. Among these, titanate compounds were the most studied [$BaTiO_3$ and Pb(Ti,Zr)O_3].[4–6] To the best of our knowledge, the microwave hydrothermal synthesis of sodium and potassium niobates has never been reported.

[a] Instituto de Química – Universidade Estadual Paulista (UNESP),
Rua Prof. Francisco Degni, s/n, 14801-970, P. O. Box 355 Araraquara, SP, Brazil
Fax: +55-16-3301-6692
E-mail: amauri_jp@yahoo.com.br

Although sodium niobate ($NaNbO_3$) has been successfully obtained by the reaction of Nb_2O_5 and NaOH through conventional hydrothermal techniques,[7,8] more studies are necessary to understand its crystallization under the hydrothermal environment, as there is just one study about the structural evolution of the products of this reaction.[9] Moreover, a study based on the influence of synthetic parameters on the structure and morphology of the obtained products has never been performed.

$NaNbO_3$ possesses antiferroelectric behavior at room temperature and has the greatest number of polymorphic transformations in the perovskite-structured class of compounds.[10] The lack of spontaneous polarization in this material is the main reason for the low interest shown by researchers. However, two recent important findings about this compound have attracted the attention of chemists. The use of (001) oriented particles of this antiferroelectric material as a template during the sintering of (Na,K,Li)NbO_3 lead-free-based ceramics allowed the production of texturized ceramics with piezoelectric properties comparable to PZT properties.[11] Moreover, the recent production of disodium diniobate hydrate ($Na_2Nb_2O_6{\cdot}H_2O$) microfibers, which can serve as sandia octahedral molecular sieves (SOMS), by conventional hydrothermal methods also awoke interest in this material.[12] These fibers, being microporous, can be used as ionic exchangers mainly with cations having a valence of 2+ (Sr^{2+} radioactive cations for example).

The proposal to study the microwave-assisted hydrothermal synthesis of $NaNbO_3$ through the reaction of niobic acid ($Nb_2O_5{\cdot}nH_2O$) and sodium hydroxide (NaOH) is now

being fulfilled. The precipitation of niobic acid in the solution medium can be achieved by cleavage of the niobium ammonia oxalate complex $[NH_4NbO(C_2O_4)_2(H_2O)_2\text{-}(H_2O)_n]$ through pH alteration. A study of the critical parameters such as reaction time and reactant concentration in the resultant insoluble products is announced. By changing the concentrations of NaOH and Nb^{5+} and the reaction time, it was possible to determine the exact conditions to produce specific types of products. Moreover, the use of $Nb_2O_5{\cdot}nH_2O$ instead of Nb_2O_5 as the niobium raw material and the presence of the NH_3 volatile agent in the reaction medium can be used to cause considerable differences in the synthesis.

Results and Discussion

Investigation of Reaction Times

Seven different reaction times were used to provoke the reaction between $Nb_2O_5{\cdot}nH_2O$ and NaOH under hydrothermal conditions. The collection of the precipitate was done 40, 70, 100, 160, 280, 520, and 760 min after initiating the synthesis. Up to 40 min, the desired temperature had not been attained, as the system was still heating. The pressure of the system reached a maximum of 1.72 ± 0.103 MPa after 50 min. The total weight of products recovered after washing and centrifuging suggested that the quantity of reactant remaining in the water after completion of the reaction was minimal.

The XRD patterns of the products recovered after these times are shown in Figure 1. According to these results, the $NaNbO_3$ phase is achieved at 100 min. The same structure of $NaNbO_3$ was obtained after 100, 160, 280, 520, and 760 min. The precipitate formed was identified as an orthorhombic structure (P*bcm* space group) with the following cell parameters: a = 5.506 Å, b = 5.566 Å, c = 15.520 Å (ICSD 23239). This same structure was produced by Santos et al. through the reaction of NaOH with Nb_2O_5 at high molar ratios of $NaOH/Nb_2O_5$ (67).[7] For the products collected after 40 min, the presence of the structure corresponding to $Na_2Nb_2O_6{\cdot}H_2O$ microfibers was identified. This crystalline structure was recently established by Xu et al.[13] as being a monoclinic phase (space group *C2/c*), with cell parameters: a = 17.0511(9) Å, b = 5.0293(2) Å, c = 16.4921(9) Å, and β = 113.942(2)°. The same structure was obtained at 200 °C by Zhu et al., who studied the evolution of the reaction between NaOH and Nb_2O_5 by using the conventional hydrothermal method.[9] The authors described $Na_2Nb_2O_6{\cdot}H_2O$ as being an intermediary metastable phase in the crystallization of $NaNbO_3$. For products obtained after 70 and 100 min, a coexistence of $NaNbO_3$ and $Na_2Nb_2O_6{\cdot}H_2O$ was found, wherein the formation of $NaNbO_3$ occurred as the $Na_2Nb_2O_6{\cdot}H_2O$ phase was consumed.

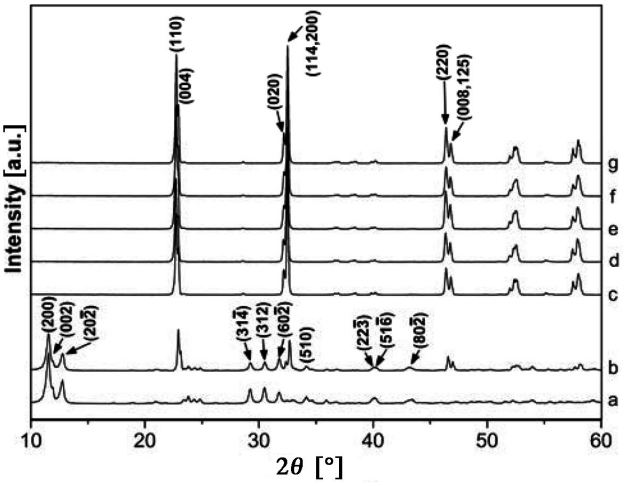

Figure 1. XRD of the products for different times of synthesis: (a) 40, (b) 70, (c) 100, (d) 160, (e) 280, (f) 520, and (g) 760 min. Major peaks of $Na_2Nb_2O_6{\cdot}H_2O$ and $NaNbO_3$ are indexed.

The SEM images of the products are shown in Figure 2. The exclusive presence of $Na_2Nb_2O_6{\cdot}H_2O$ fibers with an average diameter of 200 nm was evidenced in the products obtained after 40 min (Figure 2a). For the products obtained after 100 min, the unique presence of $NaNbO_3$ cubic-like particles was identified, although an increase in their sizes was observed. This later-stage-growth process is associated with a coarsening process (or Ostwald ripening), mainly described by Lifshitz, Slyozov, and Wagner[14,15] and commonly called the LSW theory. This process could be briefly described as the growth of a particle through the dissolution of similar ones with minor sizes, and their subsequent deposition on the particle surface. The process happens spontaneously, in an attempt to decrease the total surface energy. Particles with a radius smaller than the critical radius ($r < r_c$) suffer dissolution, whereas particles with a larger radius have a tendency to undergo deposition, and consequently, they grow. The critical radius changes with the solute concentration and, consequently, with the reaction time as well. This phenomenon happens independently from the particle-growth process that occurs just after nucleation, wherein the ions present in solution are deposited on the solid. By considering a significant decrease in the water viscosity under hydrothermal conditions, the diffusion of the solute should be very fast and, consequently, coarsening should not be diffusion-controlled as it is commonly described by LSW-based theories.[16] A recent model for this process suggested that a reversible dissolution/deposition mechanism rules the coarsening of $BaTiO_3$ particles under hydrothermal synthesis.[17,18] In this model, the authors established a linear crescent relationship between r_a (average radius) and t (time) for the growth curves. As depicted in Figure 2b,c, a size growth occurred as a function of time, and the particle size distribution narrowed. However, the cubic-like particles produced after reactions times of 280, 520, and 760 min did not obey the linear relationship between r_a and t, as a significant increase in their sizes (Figure 2b,c) was not seen. Possibly, this deviant behavior

is related to the high NaOH concentrations used in this work. Adsorption of OH^- on the particle surface can hinder the posterior deposition on the solid, once there is a dissolution/deposition mechanism ruling the coarsening process. As the authors used low concentrations of $BaOH_2$ (1.68 mol dm^{-3}) for the synthesis of $BaTiO_3$, this effect was not observed.[18]

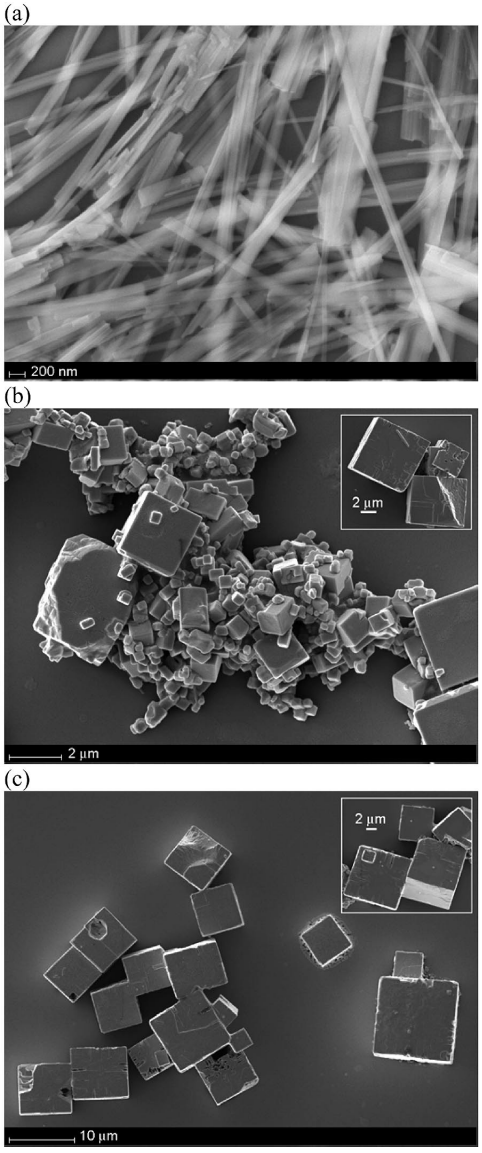

Figure 2. SEM images of the products for different reactions times: (a) 40, (b) 160, and (c) 760 min. The insets in (b) and (c) show cubic-particles obtained after 280 and 520 min of synthesis, respectively.

Investigation of Reactant Concentrations

The structural characterization of the products was accomplished through XRD (Figure 3). Poor crystallinity was visualized in the products obtained with low concentrations of NaOH (Figure 3, products 1 and 2). For intermediary concentrations of this reactant (Figure 3, products 3 and 4), the main formation of $Na_2Nb_2O_6{\cdot}H_2O$ microfibers was evidenced, although a small quantity of the $NaNbO_3$ phase was found in product 4. In products 4 to 7, the $Na_2Nb_2O_6{\cdot}H_2O$ monoclinic phase was consumed as a consequence of the formation of orthorhombic $NaNbO_3$. Product 7 presented the unique presence of $NaNbO_3$ powders.

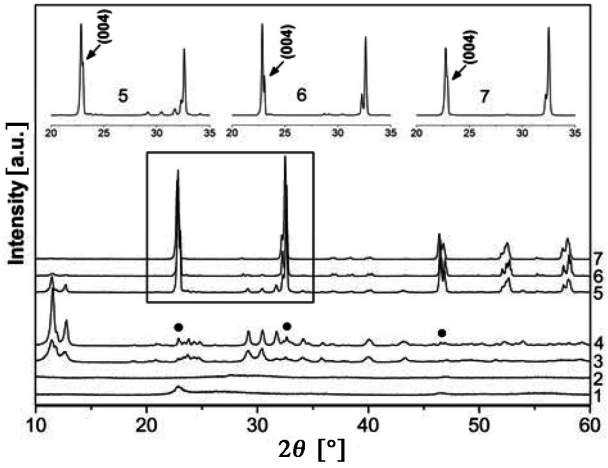

Figure 3. XRD of the products obtained after 100 min starting from different precursor ratios. The numbers indicate the same %-wt composition as given in Figure 9. The patterns of products 5, 6, and 7 are expanded in the inset; major peaks of the $NaNbO_3$ orthorhombic phase are indicated by ●.

By knowing the OH^- catalytic role in hydrothermal synthesis and by raising its concentration in the reaction medium for conditions 1 to 6, different kinetics were expected for each synthesis. The OH^- ion, a mineralizing agent, assists the reactants mass transport during the seed formation in the crystallization process, and it also contributes to the crystal nucleation and its growth process; this results in the acceleration of the reaction.[19] Because the $Na_2Nb_2O_6{\cdot}H_2O$ microfibers correspond to an intermediary phase in this reaction, their presence was restricted to medial concentrations of OH^-, whereas a large amount of $NaNbO_3$ particles are present for greater concentrations of this ion. In this context, it is reasonable to say that the effect produced by raising the OH^- concentration in the resultant products could be parallelly associated with an increase in the reaction time. However, as previously mentioned the high OH^- concentration could act differently on the later-stage coarsening process and interfere in the morphology of the resulting products.

During the conversion of $Na_2Nb_2O_6{\cdot}H_2O$ microfibers into $NaNbO_3$ cubes, preferentially oriented patterns were observed for products containing mixtures of these two phases. As seen in the insets of Figure 3, product 5 crystallized with an orientation in the (004) crystalline plane. In products 5 to 7, the loss of this orientation was observed and a normal polycrystalline XRD pattern was evidenced. This natural behavior during this conversion reaction can be successfully used to obtain $NaNbO_3$ templates, which can be used in texturing applications, such as templated grain growth (TGG) or reactive templated grain growth (RTGG) methods for example.

The evolution of the particles morphology obtained in the syntheses of 1 to 7 is shown in Figure 4. Noncrystalline products 1 and 2 (Figure 4a) did not present a defined morphology, and they were characterized as agglomerates of minor particles. The crystallization of the microfibers occurred in huge agglomerates (Figure 4b), which suffer a posterior segregation according to their growth and with a consequent decrease in surface energy (Figure 4c). A heterogeneous growth occurs along their length once a variation in the diameter size of the same fiber can be observed (Figure 4e). The crystallization of cubic-like particles with micrometers of size was visualized for product 7 (Figure 4d).

In an attempt to identify the different structures formed during the evolution of the reaction toward $NaNbO_3$ crystallization, the products were analyzed by Raman spectroscopy. The identification of the Raman vibration modes for these products can be done on the basis of two different symmetry considerations. First, a factor group correlation between the point group symmetries of each atom in the unit cell, and the lattice space group symmetry (*Pbcm* for $NaNbO_3$ and *C2/c* for $Na_2Nb_2O_6.H_2O$) originates the vibrational modes of each atom separately.[20] Second, the internal modes originating from the NbO_6 octahedron (O_h symmetry) and the lattice transitional modes of the remaining cations motion are considered.[21] The latter hypothesis is based on the stronger Nb–O interactions occurring in the NbO_6 coordination octahedron than in the remaining ones. The accuracy of this proposition is confirmed by similar vibrational spectra for different lattice structures containing the NbO_6 unit ($NaNbO_3$, $KNbO_3$, $LiNbO_3$).[22,23]

The vibrations associated to the Raman scattering for products 1, 2, 3, 4, and 7 are show in Figure 5. The NbO_6

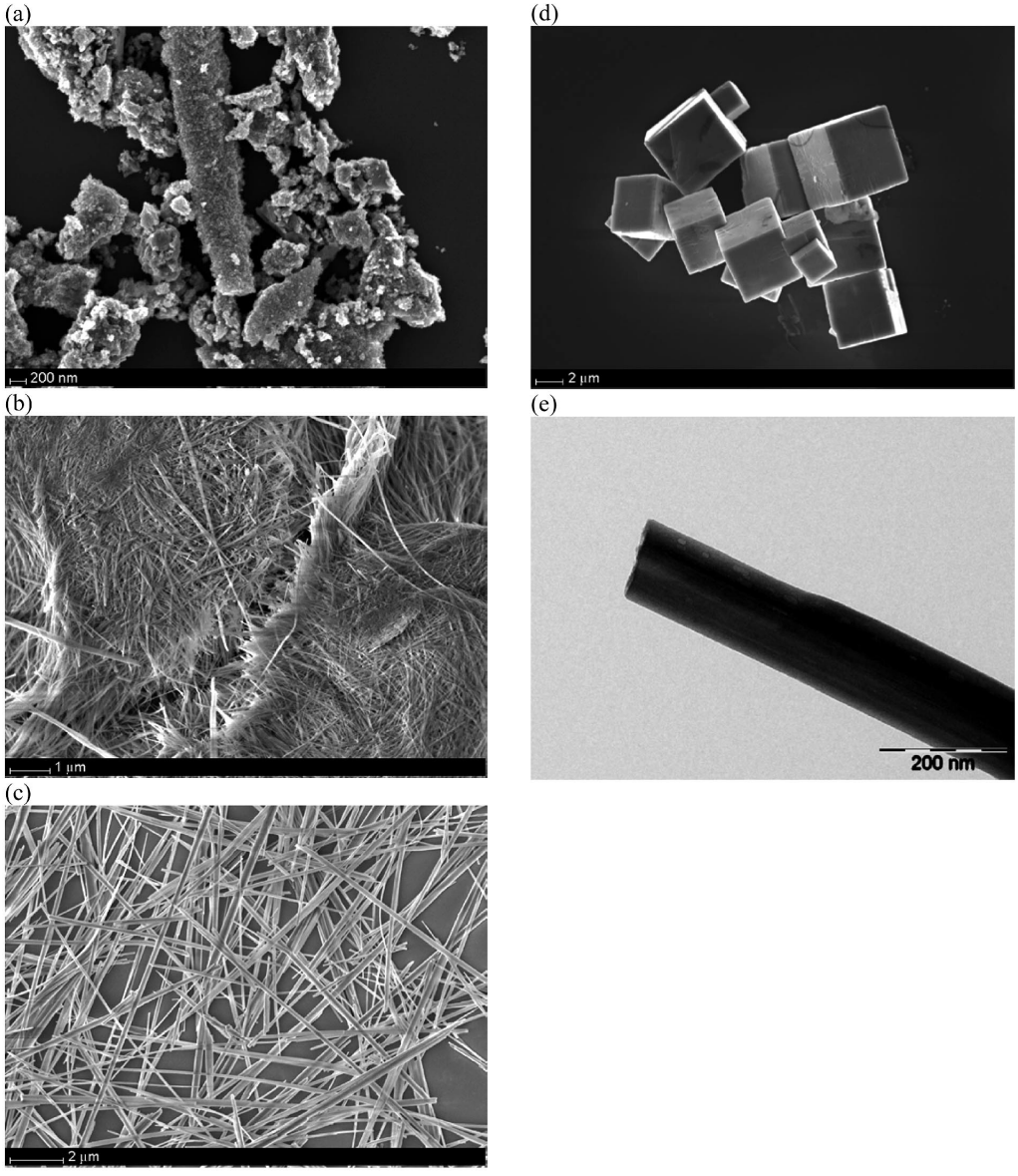

Figure 4. SEM images of the products obtained after 100 min for different precursors ratios: Products (a) 1, (b) 3, (c) 4, and (d) 7; (e) TEM image of a $Na_2Nb_2O_6{\cdot}H_2O$ microfiber produced under conditions 5.

octahedron with O_h point group symmetry has 15 vibrational modes: $1A_{1g}(\nu_1) + 1E_g(\nu_2) + 2F_{1u}(\nu_3, \nu_4) + F_{2g}(\nu_5) + F_{2u}(\nu_6)$. The A_{1g}, E_g, and F_{2g} modes are Raman active, F_{1u} is infrared active, and F_{2u} is inactive. The spectrum of product 1 is similar to that reported for $Nb_2O_5{\cdot}nH_2O$,[22] which is characterized by modes originating from the distorted NbO_6, NbO_7, and NbO_8 polyhedra. This fact confirms the presence of noncrystalline $Nb_2O_5{\cdot}nH_2O$ in this product. The spectra of products 3 and 7 are very similar to those of $Na_2Nb_2O_6{\cdot}H_2O$[24] and $NaNbO_3$,[22,23] respectively, although Zhu et al. presented a different spectrum for $NaNbO_3$.[9] The spectrum of product 4 contains a mixture of vibrational modes that can be attributed to $Na_2Nb_2O_6{\cdot}H_2O$ and $NaNbO_3$. For these products, the bands below 500 cm^{-1} were assigned to the Nb–O–Nb bending modes F_{1u} (ν_4), F_{2g} (ν_5), and F_{2u} (ν_6), which are closely related to the local symmetry. Bands at 180–183 cm^{-1} were assigned to the F_{2u} mode, those at 215–276 cm^{-1} to the F_{2g} modes, and those at 375–378 and 427–432 cm^{-1} to the antisymmetric bending mode F_{1u}. Although F_{2u} is an inactive mode and F_{1u} is only IR active, their appearance in the Raman spectrum occurs as a consequence of the multiple unit cell interactions that are responsible for the relaxation in the selection rules. The translational motion of the Na cations against the NbO_6 octahedron is associated with the 141–144 and 122 cm^{-1} bands.[21] A Nb–O–Nb bending mode (F_{2g}) at 459 cm^{-1} was once predicted and observed in the spectrum of the $Nb_6O_{19}^{8-}$ and $Ta_6O_{19}^{8-}$ ions.[25] As expected, this mode appears at this high wavelength (459 cm^{-1}) only for $Na_2NbO_6{\cdot}H_2O$ (products 3 and 4) and product 2; this may be related to the presence of edge-shared NbO_6 octahedra units in these three powders.

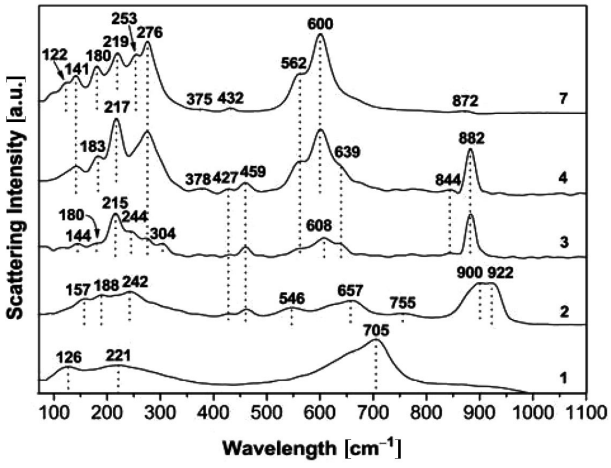

Figure 5. Raman spectra of products 1, 2, 3, 4, and 7.

Wavelengths above 500 cm^{-1} in the spectra of products 3, 4, and 7 (Figure 5) are related to the stretching modes A_{1g} (ν_1), E_g (ν_2), and F_{1u} (ν_3). The intense band at 882 cm^{-1} observed for product 3 is assigned to a Nb=O stretching vibration, possibly the A_{1g} mode, which is related to the shortest Nb–O bond length in $Na_2Nb_2O_6{\cdot}H_2O$. The shorter the bond length, the higher its vibrational frequency.[26] For $NaNbO_3$, the same mode occurs at 600 cm^{-1}. The less-intense band at 872 cm^{-1} in the spectrum of product 7 is related to the Nb–O–Nb antisymmetric stretching mode F_{1u}.[21,22] The stretching mode E_g appears at 562 cm^{-1}. The Raman spectrum of product 2 was very similar to that of $Na_2Nb_2O_6{\cdot}H_2O$. A hypothesis that this product holds NbO_6 octahedral units with edge-sharing structures is very plausible, if the modes present in the spectrum resemble those in the spectrum of product 3. Therefore, the rupture of the corned-shared NbO_7 and NbO_8 polyhedra present in $Nb_2O_5{\cdot}nH_2O$ is confirmed. It is quite possible that the most intense bands at 900 and 922 cm^{-1} are assigned to A_{1g} Nb=O stretching modes of different bond lengths. The displacement of the A_{1g} mode to lower wavelength values in the spectra of products 2 to 7 (922 → 882 → 600 cm^{-1}) is closely related to the higher symmetry in the NbO_6 octahedron, which means a rise of structural order. Moreover, the presence of a greater amount of bands above 500 cm^{-1} in product 2 (546, 657, 755, 900, and 922 cm^{-1}) is also related to a less-homogeneous distribution of the Nb–O bond lengths, as each of these modes originate from different bond lengths.

The local environment of sodium in products 1, 2, 3, 4, and 7 can be determined by ^{23}Na MAS-NMR spectra (Figure 6). The presence of Na cations in all products is confirmed through the resonance detected in the spectra. Quite broad peaks with maxima at –3.9 (A) and –9.9 ppm (B) are seen for products 1 and 2, respectively. A splitting of peak B into C and D at –8.6 and –13.9 ppm, respectively, and the appearance of a new one at –45.9 ppm (E) characterizes the resonances of Na in $Na_2NbO_2O_6{\cdot}H_2O$ microfibers (product 3). As the conversion of the microfibers into $NaNbO_3$ occurs, from products 3 to 7, peaks I (–10.1 ppm) and J (–28.3 ppm) rise upon the previous ones. The spectrum of product 4 possesses four peaks with maxima at –8.3 (F), –13.6 (G), –28.3 (J), and –46.7 ppm (H), which represents the responses of three Na sites in $Na_2NbO_2O_6{\cdot}H_2O$ and two Na sites in $NaNbO_3$. The appearance of broad peaks in products 1 and 2 reveals the presence of poorly crystallized solids; this was already confirmed by XRD (Figure 3). Even without the occurrence of a reaction between Na^+ and $Nb_2O_5{\cdot}nH_2O$, the presence of sodium was identified in product 1, which suggests that incorporation of Na cations into the $Nb_2O_5{\cdot}nH_2O$ structure occurred during its precipitation, with cleavage of the ammonia complex. The displacement of the maximum point from –3.9 to –9.9 ppm indicates the presence of fewer protected Na sites in product 2 relative to those present in product 1. The three characteristic Na sites in $Na_2NbO_2O_6{\cdot}H_2O$ are associated with peaks C, D, and E, wherein two of them are rounded by six oxygen atoms in a octahedral coordination (Na1 and Na2), and the remaining one is located in an extraframework position (Na3) coordinated by four oxygen atoms in a distorted square-planar symmetry.[13] The lower symmetry of the Na3 extraframework site causes a greater chemical shift for this site relative to those of Na1 and Na2. In this way, peak E can be assigned to the Na3 site, whereas the overlapped resonance represented by peaks C and D

can be assigned to Na1 and Na2, respectively. As a result of the second-order quadrupolar interaction between the Na nuclei and the electromagnetic radiation, the ^{23}Na MAS-NMR technique produces rather anisotropic spectra. Because there is just a slight difference between the octahedral environments of Na1 and Na2, the differentiation of each one of them through MAS-NMR becomes very difficult. However, by using the multiple quantum magic-spinning technique (MQMAS), these two sites could be distinguished in a previous study that confirmed the subtle difference between their resonances.[9] Sodium cations occupy two different sites in the $NaNbO_3$ crystalline structure (ICSD 23239); the first one is rounded by three oxygen atoms in a triangle (Na 1) and the other is rounded by four oxygen atoms in a tetrahedral coordination (Na2). Because Na1 is less protected than that with the tetrahedral coordination, peak J can be assigned to Na1, whereas peak I can be assigned to the Na2 site.

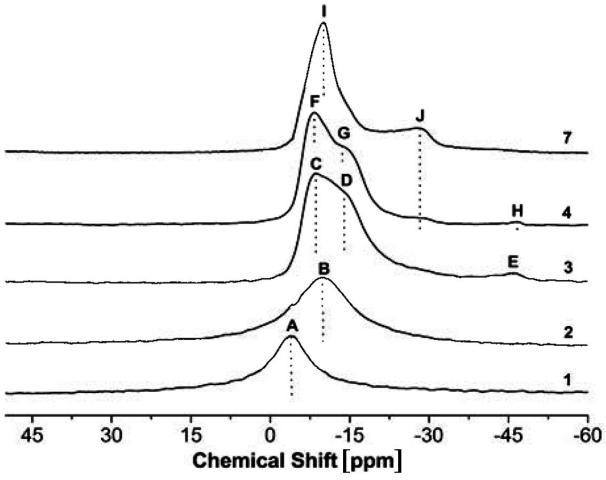

Figure 6. ^{23}Na MAS-NMR spectra of products 1, 2, 3, 4, and 7.

Reaction between $Nb_2O_5{\cdot}nH_2O$ and Na^+ in Alkaline Medium

The first step of the reaction consists of the rupture of the corner-shared NbO_7 and NbO_8 polyhedra in $Nb_2O_5{\cdot}nH_2O$ and the consequent formation of Lindqvist ions ($Nb_6O_{19}^{8-}$),[8] which consists of an edge-sharing structure with six octahedra of NbO_6 [Reaction (1)]. Subsequently, XRD results (Figure 3) and Raman spectra (Figure 5) indicated the formation of a poorly crystallized sodium niobium oxide, possibly hydrated, consisting of edge-sharing NbO_6 octahedra. This solid probably maintains the Nb_6O_{19} units present in solution and, consequently, incorporates sodium cations and water molecules into its structure, such as $Na_7(H_3O)Nb_6O_{19}(H_2O)_{14}$ for example.

$$3\ Nb_2O_5{\cdot}H_2O + 8\ OH^- \rightarrow Nb_6O_{19}^{8-} + 7\ H_2O \quad (1)$$

The conversion of this intermediate into $Na_2Nb_2O_6{\cdot}H_2O$ occurs with an ordering of the NbO_6 edge-shared octahedra, which means a more homogeneous distribution of Nb–O bond lengths and the arrangement of Na cations in three structural sites (Na1, Na2, and Na3). The water molecules that are possibly present in the unit cell of the intermediary product are maintained in the microfiber structure. In the final step, the production of the $NaNbO_3$ phase is a result of another increase in the order of the NbO_6 octahedra, followed by a structural rearrangement, which is responsible for the formation of distorted NbO_6 corner-shared octahedra and two Na sites, with triangular and tetrahedral coordinations. Water molecules are consequently liberated in this reaction [Reaction (2)].

$$Na_2Nb_2O_6{\cdot}H_2O \rightarrow 2\ NaNbO_3 + H_2O \quad (2)$$

Comparison of Nb Precursor in $NaNbO_3$ Production

The reaction was performed at 200 °C for 760 min, but 40 min of that time was required to reach 200 °C. The first difference appears in the structure of $NaNbO_3$. As seen in Figure 7a, the use of niobium pentoxide (Nb_2O_5) as a precursor provoked the production of a monoclinic phase with lattice parameters: a = 3.91140 Å, b = 3.88130 Å, c =

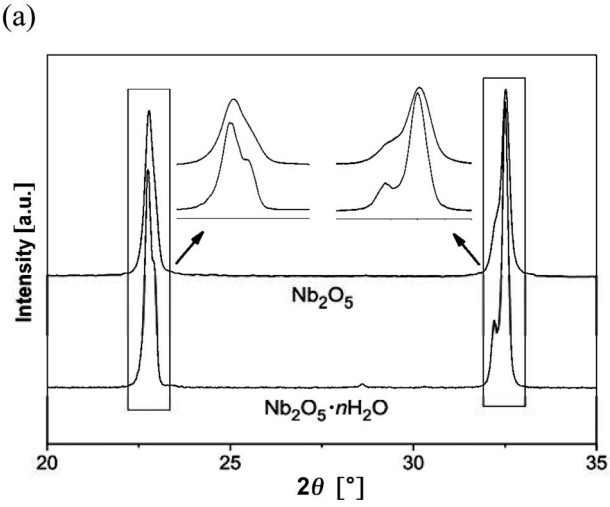

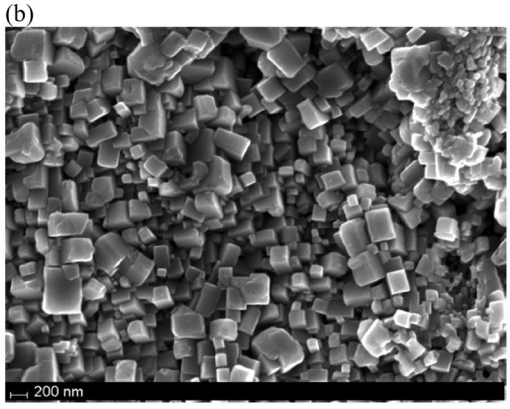

Figure 7. (a) Comparison between the XRD results of products obtained after a reaction time of 760 min with different Nb precursors, (b) SEM images of $NaNbO_3$ powders produced at 200 °C after 760 min by using Nb_2O_5 as the Nb raw material.

3.91140 Å, and β = 90.620° (ICSD 28565), which is different from that observed for the products obtained through the reaction of $Nb_2O_5{\cdot}nH_2O$ with Na^+ with an identical reaction time (Figure 1g). The SEM image (Figure 7b) clearly shows a different size and shape of the cubes relative to those obtained in the first part of this work (Figure 2c). The particles synthesized with niobium ammonia oxalate were greater in size, whereas the Nb_2O_5 precursor afforded powders varying from 200–500 nm in size, and $Nb_2O_5{\cdot}nH_2O$ promoted the formation of micrometer-sized cubic-like particles; the latter are the most attractive for template use. By considering the greater pressure in the synthesis containing the ammonia complex precursor over that containing niobium pentoxide (1.72 vs. 1.03 MPa), as a result of the presence of volatile NH_3 in the first, it is understandable why these particles are bigger once the mass transfer is enhanced with pressure. Another point to be considered is the bypassing of the hydroxylation step in the $Nb_2O_5{\cdot}nH_2O$ precursor, which has its dissolution facilitated.

Structural Refinement of the $Na_2Nb_2O_6{\cdot}H_2O$ Microfibers

The product collected after a reaction time of 40 min, which exclusively contained microfibers (Figure 1a), was subjected to Rietveld[27] refinement. The starting parameters used were based on the $Na_2Nb_2O_6{\cdot}H_2O$ monoclinic phase (Table 1). The general structure analysis system (GSAS)[28] with the graphic user interface (EXPGUI)[29] was used to conduct the experiment.

Bond lengths in the range 0–2 Å are shown in Figure 8. On the basis of refinement indices of 1.7% for R_{Bragg}, 1.3% for S, and 12.4% for R_{wp}, the cell parameters obtained were: a = 17.0550(9) Å, b = 5.0286(4) Å, c = 16.4981(9) Å, and β = 113.94°. This $Na_2Nb_2O_6.H_2O$ monoclinic phase possesses three types of sites for the Na atoms, as cited before. Two sodium cations at the Na3 site have distances less than 1.0 Å [d = 0.9569(1) Å] between them; this is the shortest interaction in the structure, and it is almost half of the shortest Nb–O bond length (Figure 8). Because there are no predominant attractive interactions between these two positive Na atoms, this proximity creates a high electrostatic repulsion, which results in the most unstable interaction in the structure. Therefore, in suspensions of these microfibers in solutions containing determined cations, under normal conditions of temperature, these Na cations at the Na3 site have a tendency to be easily substituted by other cations to decrease the energy of the system. As expected, tests indicated that there is greater selectivity for 2+ valence rather than 1+, because the prior provides a more stable structure due to the absence of electrostatic repulsion between two nuclei as just one cation is present at the site. Previous studies have already evidenced a great selectivity for Ba^{2+}, Pb^{2+}, Co^{2+}, Sr^{2+}, Ni^{2+}, Zn^{2+}, and Cd^{2+}.[30]

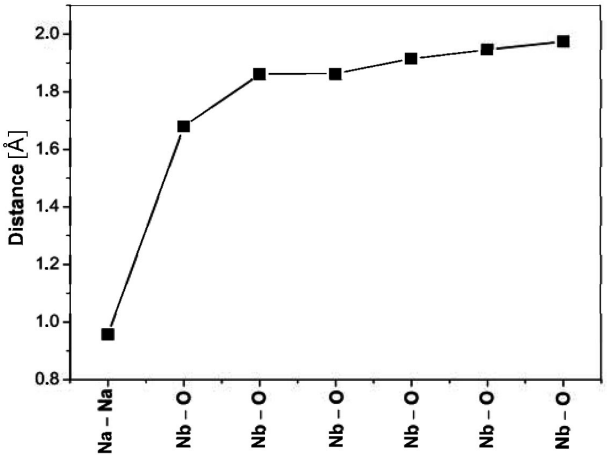

Figure 8. Bond lengths between 0 and 2 Å in the $Na_2Nb_2O_6{\cdot}H_2O$ monoclinic unit cell.

Conclusions

The use of microwave-assisted hydrothermal synthesis for the production of pure phases of $NaNbO_3$ and $Na_2Nb_2O_6{\cdot}H_2O$ by using niobic acid as the Nb raw material was successfully achieved. This antiferroelectric material ($NaNbO_3$) and its intermediary phase ($Na_2Nb_2O_6{\cdot}H_2O$) were obtained after reaction times of 100 and 40 min, respectively. The time of reaction and the concentration of the reactants can control the specific production of one of these two compounds. During the evolution of the reaction between $Nb_2O_5{\cdot}nH_2O$ and Na^+, a poorly crystallized solid

Table 1. Structural parameters of the $Na_2Nb_2O_6{\cdot}H_2O$ monoclinic phase.

Structure	Atom	Site	x	y	z	SOF
$Na_2Nb_2O_6{\cdot}H_2O$	Na1 I+	8f	0.3347(5)	–0.3662(11)	0.7337(5)	1
Space group $C2/c$	Na2 I+	4e	1/2	0.1399(18)	3/4	1
(Z = 8)	Na3 I+	8f	0.2628(13)	0.2876(35)	0.0121(12)	0.5
a = 17.0511(9) Å	Nb1 V+	8f	0.4052(1)	0.0456(4)	0.9057(1)	1
b = 5.0293(2) Å	Nb2 V+	8f	0.5325(1)	0.5494(4)	0.9149(1)	1
c = 16.4921(9) Å	O1 2–	8f	0.4615(5)	–0.2541(19)	–0.0039(7)	1
β = 113.942(2)°	O2 2–	8f	0.4773(7)	–0.1478(17)	0.8490(8)	1
ICSD: 55415	O3 2–	8f	0.4201(7)	0.3588(19)	0.8500(7)	1
	O4 2–	8f	0.3777(6)	0.2492(19)	0.9930(6)	1
	O5 2–	8f	0.6005(6)	0.4178(18)	0.8607(6)	1
	O6 2–	8f	0.3018(6)	–0.0937(19)	0.8374(7)	1
	O7 2–	8f	0.1993(7)	0.5054(20)	0.8687(7)	1

with edge-shared NbO_6 octahedra units is obtained as a precursor of $Na_2Nb_2O_6{\cdot}H_2O$ microfibers. A structural ordering of this sodium niobium oxide results in the formation of the microfibers, which are subsequently converted into $NaNbO_3$ cubes through the rupture of the NbO_6 edge-shared structures. During this last conversion, it was found that a tendency for oriented crystallization resulted in the formation of (001) oriented cubic-like particles of $NaNbO_3$, which could be successfully used for templated texturization processes (TGG or RTGG). The use of the niobium ammonia oxalate as a Nb raw material allowed bigger particles (>5 μm) to be formed, which are more desirable for templated grain growth applications. Therefore, with the interest in $Na_2Nb_2O_6{\cdot}H_2O$ as an ionic exchanger and in $NaNbO_3$ templates for texturing applications, the reaction between $Nb_2O_5{\cdot}nH_2O$ and NaOH through a microwave-assisted hydrothermal method presents itself as an extremely fast and efficient option for their preparation.

Experimental Section

Reagents and Methods: The synthesis of $NaNbO_3$ powders from NaOH (Mallinckrodt, 99%) and $NH_4NbO(C_2O_4)_2(H_2O)_2(H_2O)_n$ (CBMM, 98%) was performed in decarbonated water as a medium. The microwave-assisted hydrothermal syntheses were carried out with a MARS-5 digestion system in a Teflon vessel model XP-1500 (CEM Corp.). The microwave digestion system uses a frequency of 2.45 GHz and can operate at a power level between 0–100% at 300, 600, or 1200 W. The wattage used in these experiments was 300 W. The X-ray powder diffraction patterns of the synthesis products were measured with a Rigaku Rink 2000 instrument, equipped with a rotating anode, operating at 50 KV and 100 mA, with Cu-K_α radiation in the range 2θ = 10–90°. The morphology of the resultant products was analyzed by scanning electron microscopy (Zeiss, Supra 35) with a field emission gun and by transmission electron microscopy (Philips, CM-200). The Raman scattering spectra in the range 70–2000 cm^{-1} was obtained in a Fourier Transform Spectrograph (Bruker FT-Raman RFS100/S) by using a 1064-nm Nd:YAG laser with 150 mW of nominal power. ^{23}Na NMR spectra in magic spinning angle mode (MAS-NMR) were collected with a Varian Inova spectrometer operating at a magnetic field of 7.04 T, with a 7-mm probe (CP-MAS). The ^{23}Na resonance frequency was 79.3 MHz. The spectra were recorded with a π/3 (2μs) pulse sequence with a delay of 4 s and a spinning speed of 6 kHz. Chemical shift reference (δ =0 ppm) was based on a 1.0-M NaCl solution.

Reaction Time Study: In order to discover an appropriate time to obtain $NaNbO_3$, a study to determine the time dependence in the resultant products was done. A first solution of Nb^{5+} (0.3 mol dm^{-3}) was made by dissolving the proper quantity of niobium ammonia oxalate in deionized water. The second solution of sodium hydroxide (15.0 mol dm^{-3}) was also prepared in deionized water. Because of the instability of the niobium oxalate complex in alkaline media, the merging of the first solution (12.5 mL) with the second (12.5 mL) resulted in a NaOH solution (7.5 mol dm^{-3}, 25 mL) with Nb precipitated (0.348 g) as $Nb_2O_5{\cdot}nH_2O$. This resulting solution was placed in Teflon vessels and put into the microwave hydrothermal system. The synthesis was promoted at 200 °C after a heating time of 40 min to achieve this desired temperature. The products of the reactions after different times were collected, washed, separated by centrifuging, and finally dried. The morphological and structural differences of the $NaNbO_3$ powders obtained by the two different Nb raw materials were also evaluated. For this, Nb_2O_5 (99.5% Aldrich, 0.498 g) was added to a NaOH solution (7.5 mol dm^{-3}, 25 mL). The concentration of NaOH, volume of water, quantity of available Nb in the vessel, and the heat scheme used was exactly the same as that used in the preparation of $Nb_2O_5{\cdot}nH_2O$. In this way, the differences in the use of niobic acid ($Nb_2O_5{\cdot}nH_2O$) instead of common niobium pentoxide (Nb_2O_5) could be analyzed.

Precursor Concentration Study: Variations in the concentrations of NaOH and $NH_4NbO(C_2O_4)_2(H_2O)_2(H_2O)_n$ in the starting solution would result in the formation of different products. In this way, several solutions (25 mL) containing niobium ammonia oxalate and sodium hydroxide at different concentrations were subjected to the microwave hydrothermal reaction. The samples were prepared by merging the solutions of $NH_4NbO(C_2O_4)_2(H_2O)_2(H_2O)_n$ and NaOH at several concentrations each. As described above, niobium was present in the medium as $Nb_2O_5{\cdot}nH_2O$ for all samples. In the ternary phase diagram shown in Figure 9, we can observe the explored area used for the syntheses. The lines seen in the diagram correspond to fixed ratios between two of the reactants. The conditions represented by numbers 1 to 6 were made up with a ratio of 21:1 between H_2O/niobium oxalate percentages, whereas conditions 6 and 7 were made up with a fixed ratio of 3:3 between H_2O and NaOH. The lowest concentration of NaOH was 0.1 M (condition 1), whereas the highest was 7.5 M (condition 6 and 7). The syntheses were also undertaken at 200 °C with the same heat scheme as described above. For conditions 4, 5, and 6, the pressure stabilized at ca. 1.48 MPa, whereas for condition 3 it stabilized at 1.58 MPa, and all conditions has a small variation of ±0.0689 MPa. Conditions 1 and 2 achieved a stabilized pressure of ca. 1.79 MPa, whereas 7 stabilized at ca. 1.72 MPa, and all varied around ±0.103 MPa.

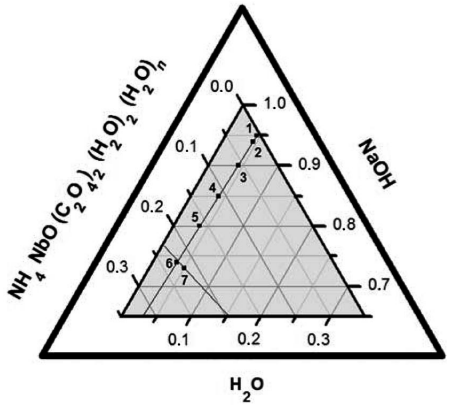

Figure 9. Explored area of the $NH_4NbO(C_2O_4)_2(H_2O)_2(H_2O)_n$/$H_2O$/NaOH ternary diagram. The ratios in %-wt are given as follow: (1) 4.49/95/0.510, (2) 4.42/94/1.58, (3) 4.26/90/5.74, (4) 4.00/85/11.0, (5) 3.75/80/16.25, (6) 3.50/74/22.5 and (7) 5.00/73/22.0.

Acknowledgments

This research was funded by a grant from the Fapesp Brazilian Agency.

[1] M. M. Lencka, R. E. Riman, *Chem. Mater.* **1993**, *5*, 61–70.
[2] C. Sun, X. Xing, J. Chen, J. Deng, L. Li, R. Yu, L. Qiao, G. Liu, *Eur. J. Inorg. Chem.* **2007**, 1884–1888.

[3] A. Magrez, E. Vasco, J. W. Seo, C. Dieker, N. Setter, L. Forró, *J. Phys. Chem. B* **2006**, *110*, 58–61.
[4] S.-F. Liu, I. R. Abothu, S. Komarneni, *Mater. Lett.* **1999**, *38*, 344–350.
[5] I. R. Abothu, S.-F. Liu, S. Komarneni, Q. H. Li, *Mater. Res. Bull.* **1999**, *34*, 1411–1419.
[6] B. L. Newalkar, S. Komarneni, H. Katsuki, *Mater. Res. Bull.* **2001**, *36*, 2347–2355.
[7] I. C. M. S. Santos, L. H. Loureiro, M. F. P. Silva, A. M. V. Cavaleiro, *Polyhedron* **2002**, *21*, 2009–2015.
[8] G. K. L. Goh, F. F. Lange, S. M. Haile, C. G. Levi, *J. Mater. Res.* **2003**, *18*, 338–345.
[9] H. Zhu, Z. Zheng, X. Gao, Y. Huang, Z. Yan, J. Zou, H. Yin, Q. Zou, S. H. Kable, J. Zhao, Y. Xi, W. N. Martens, R. L. Frost, *J. Am. Chem. Soc.* **2006**, *128*, 2373–2384.
[10] H. D. Megaw, *Ferroelectrics* **1974**, *7*, 87–89.
[11] Y. Saito, H. Takao, T. Tani, T. Nonoyama, K. Takatori, T. Homma, T. Nagaya, M. Nakamura, *Nature* **2004**, *432*, 84–87.
[12] M. Nyman, A. Tripathi, J. B. Parise, R. S. Maxwell, T. M. Nenoff, *J. Am. Chem. Soc.* **2002**, *124*, 1704–1713.
[13] H. Xu, M. Nyman, T. M. Nenoff, A. Navrotsky, *Chem. Mater.* **2004**, *16*, 2034–2040.
[14] I. M. Lifshitz, V. V. Slyozov, *J. Phys. Chem. Solids* **1961**, *19*, 35–50.
[15] C. Wagner, *Z. Elektrochem.* **1961**, *65*, 581–591.
[16] A. Baldan, *J. Mater. Sci.* **2002**, *37*, 2171–2202.
[17] W. Sun, *Acta Mater.* **2005**, *53*, 3329–3334.
[18] W. Sun, Y. Pang, J. Li, W. Ao, *Chem. Mater.* **2007**, *19*, 1772–1779.
[19] K. Byrappa, M. Yoshimura, *Handbook of Hydrothermal Technology*, Noyes Publications/William Andrew Publishing LLC, New York, **2001**, p., 351.
[20] M. N. Iliev, M. V. Abrashev, H.-G. Lee, V. N. Popov, Y. Y. Sun, C. Thomsen, R. L. Meng, C. W. Chu, *Phys. Rev. B* **1998**, *57*, 2872–2877.
[21] S. D. Ross, *J. Phys. C* **1970**, *3*, 1785–1790.
[22] J.-M. Jehng, I. E. Wachs, *Chem. Mater.* **1991**, *3*, 100–107.
[23] Y. D. Juang, S. B. Dai, Y. C. Wang, W. Y. Chou, J. S. Hwang, M. L. Hu, W. S. Tse, *Solid State Commun.* **1999**, *111*, 723–728.
[24] M. N. Iliev, M. L. F. Phillips, J. K. Meen, T. M. Nenoff, *J. Phys. Chem. B* **2003**, *107*, 14261–14264.
[25] F. J. Farrell, V. A. Maroni, T. G. Spiro, *Inorg. Chem.* **1969**, *8*, 2638–2642.
[26] F. D. Hardcastle, I. E. Wachs, *Sol. State Ionics* **1991**, *45*, 201–213.
[27] H. M. Rietveld, *Acta Crystallogr.* **1967**, *22*, 151–152.
[28] A. C. Larson, R. B. Von Dreele, *GSAS: General Structure Analysis System*, Report No. LAUR 86–748, Los Alamos National Laboratory, Los Alamos, NM, **2000**.
[29] B. H. Toby, *J. Appl. Crystallogr.* **2001**, *34*, 210–213.
[30] M. Nyman, A. Tripthi, J. B. Parise, R. S. Maxwell, W. T. A. Harrison, T. M. Nenoff, *J. Am. Chem. Soc.* **2001**, *123*, 1529–1530.

Received: October 18, 2007
Published Online: January 15, 2008

